

# Magnon-squeezing-enhanced weak magnetic field sensing in cavity-magnon system

Zheng Liu<sup>1</sup>, Yu-qiang Liu<sup>1</sup>, Yi-jia Yang<sup>1</sup>, and Chang-shui Yu<sup>1</sup>

<sup>1</sup>School of Physics, Dalian University of Technology, Dalian 116024, P.R. China

E-mail: ycs@dlut.edu.cn

May 2023

**Abstract.** Quantum noise and thermal noise are the two primary sources of noise that limit the sensitivity of weak magnetic field sensing. Although quantum noise has been widely addressed, effectively reducing thermal noise remains challenging in detecting weak magnetic fields. We employ an anisotropic elliptical YIG sphere as a magnetic field probe to establish a parametric amplification interaction of magnons and induce magnon squeezing effects. These effects can effectively suppress thermal noise in the magnon mode and amplify weak magnetic field signals from external sources. Specifically, complete suppression of thermal noise can be achieved by placing the YIG sphere in a squeezed vacuum reservoir. Our scheme has the potential to inspire advancements in thermal noise suppression for quantum sensing.

## 1. Introduction

In quantum sensing, [1–16], the performance of the system is inevitably affected by quantum noise arising from quantum fluctuations and thermal noise resulting from system thermal fluctuations [17–19]. Thus, mitigating system noise and amplifying weak signals is crucial for improved sensing performance. Recently, sensing weak magnetic fields has been extensively explored using the cavity-magnon system [20–24]. This system offers high-frequency tunability [25], high spin density [26], and a long coherence time in the magnon mode of yttrium iron garnet (YIG) spheres [27, 28]. Additionally, the ground state magnon mode (Kittel mode) of YIG spheres [29] can interact with various frequency bands of fields, including optical and microwave fields, making them excellent readout devices for detecting magnon modes [10, 30–35]. Moreover, magnons can couple with superconducting qubits, providing advantages for spin readout [36–38]. Furthermore, the coupling of magnon-phonon-spin has been achieved [39], leading to groundbreaking applications in quantum information processing. These applications include the generation of non-classical magnon states [40–43], Floquet engineering [44], magnon-driven nonreciprocal transport [45–49], and advancements in non-Hermitian quantum physics [50–53].

The sensitivity of a cavity magnon system used for weak magnetic field sensing is primarily influenced by the microwave cavity’s quantum noise and the thermal noise of the YIG sphere’s magnon mode [10, 54]. Quantum noise comprises photons’ shot noise in the microwave cavity and the backaction noise resulting from the interaction between photons and magnons. The competition between these two types of noise creates the standard quantum limit (SQL) [55] and numerous methods, such as coherent quantum noise cancellation [56–59], quadratic coupling [60, 61], quantum squeezing [62], and Non-Markovian regime [63], have already been devised to surpass SQL by reducing the quantum noise in cavity optomechanical weak force and displacement sensing. Regarding thermal noise, one could naturally consider suppressing the thermal fluctuations by lowering the environment’s temperature, for example, using a dilution refrigerator [64]. However, achieving the desired low temperature in practical sensing scenarios could be challenging. In this regard, finding other mechanisms to reduce the impact of magnon thermal noise is significant.

This paper proposes a scheme to suppress thermal noise in magnetic field sensing. We leverage the unique anisotropic fluctuations of ellipsoidal YIG spheres in traditional cavity magnetic systems to induce a parameter-amplified magnon-magnon interaction. Through this magnon squeezing interaction, we can adjust the squeezing parameters, amplify the signal response of the magnon probe, and suppress additional noise in the microwave cavity of our weak magnetic field sensing system. This approach partially suppresses thermal noise and enhances the system’s sensitivity. Furthermore, immersion of the YIG sphere in a squeezed vacuum reservoir enables complete suppression of magnon mode thermal noise. The paper is structured as follows: Section 2 presents the model and Hamiltonian of the weak magnetic field sensing scheme with our anisotropic YIG spherical cavity magnon system. In Section 3, we delve into the system’s dynamics, provide an expression for the phase quadrature output of the weak magnetic field sensing system, and scrutinize the sensor’s performance. Section ?? employs the microwave-optical wave conversion homodyne detection method to analyze the system’s output spectrum, evaluating the response, additional noise, thermal noise, and sensitivity of weak magnetic sensing. Additionally, we offer a physical mechanism to elucidate the role of squeezed vacuum reservoirs and parametric interactions in thermal noise suppression. Finally, conclusions and discussions are presented in Section ??.

## 2. Weak sensing model and Hamiltonian

The system depicted in Fig. 1 consists of an anisotropic ellipsoidal YIG sphere within a microwave cavity. Two classical pump fields drive the microwave cavity and the YIG sphere, respectively, while an external magnetic field is applied along the x-axis. At the macroscopic spin limit, the Hamiltonian of the system can be expressed using the

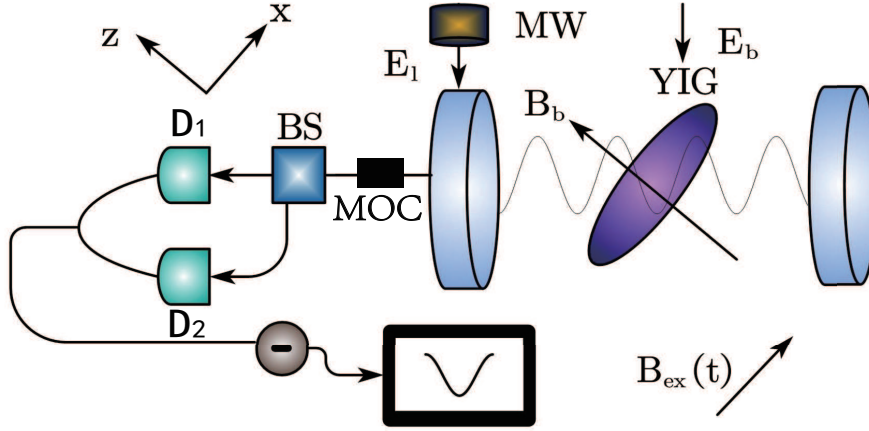


**Figure 1.** The schematic diagram of weak magnetic field sensing model. The system employs an anisotropic ellipsoidal YIG sphere as a probe to detect the external magnetic field. The microwave signal output from the cavity undergoes conversion into an optical signal via a microwave-optical wave conversion device (MOC). Subsequently, it traverses through a beam splitter (BS) before reaching two photodetectors (D1) and (D2). A subtractor is then utilized, followed by quadrature component spectrum detection, constituting a homodyne detection device. The external bias magnetic field  $B_b$  aligns with the z-axis, whereas the measured magnetic field  $B_{ex}(t)$  aligns with the x-direction. The amplitudes of the externally driven microwave field and the externally driven YIG spherical magnon mode are denoted as  $E_l$  and  $E_b$ , respectively.

Holstein-Primakoff transformations as [65–67]

$$\begin{aligned} \hat{H} = & \hbar\omega_a \hat{a}^\dagger \hat{a} + \hbar\omega_0 \hat{m}^\dagger \hat{m} + \frac{\hbar\omega_m}{2} (\hat{m}^2 + \hat{m}^{\dagger 2}) \\ & + \hbar g_0(t) (\hat{m} + \hat{m}^\dagger) (\hat{a} + \hat{a}^\dagger) + i\hbar E_l (\hat{a}^\dagger e^{-i\omega_l t} - \hat{a} e^{i\omega_l t}) \\ & - \hbar\lambda B_{ex}(t) (\hat{m} + \hat{m}^\dagger), \end{aligned} \quad (1)$$

Whereas the first two terms represent the free components of the microwave cavity field and the YIG spherical magnon mode,  $\omega_a$  and  $\omega_0$  denote the intrinsic frequencies of the cavity field and magnon, respectively. The operators  $a$  and  $m$  ( $a^\dagger, m^\dagger$ ) correspond to the annihilation (creation) operators of microwave photons and magnons. The frequency  $\omega_0$  can be modulated by a bias magnetic field  $B_b$  along the z-axis, with the gyromagnetic ratio  $\gamma = 2\pi \times 28$  GHz/T [23]. The third term describes the parametric amplification interaction due to the anisotropy of an ellipsoidal YIG sphere, where  $\omega_m = \gamma B_b - \omega_0$  stands for the corresponding anisotropic coupling coefficient, as elucidated in Refs. [66, 68]. The fourth term accounts for the dipole-dipole interaction between microwave photons and magnons. In contrast, the fifth and sixth terms denote the Hamiltonian driven by the two semi-classical pump fields. Here,  $E_l = \sqrt{2P_l \kappa_a / \hbar \omega_l}$  represents the amplitude of the pump field with frequency  $\omega_l$ , where  $P_l$  denotes the power of the microwave pump field, with  $\kappa_a$  denoting the dissipation of the microwave cavity field. Notably, the coupling strength between photons and magnons adopts time-dependent

coherent modulation, i.e.,  $g_0(t) = g_0 + 2g_0A \cos(\omega't)$ , where  $\omega'$  and  $A$  signify the coherent modulation frequency and amplitude, achievable through a Josephson parametric amplifier (JPA) to control the strength of magnon-photon coupling. Specifically, by adjusting the magnetic flux bias of the superconducting quantum interference device (SQUID) circuit in JPA, the inductance of SQUID can be modulated [10]. Here,  $g_0 = \gamma B_0 \sqrt{5N}/2$  represents the cavity magnetic coupling coefficient without time-dependent modulation, and the intensity of the microwave field is denoted by  $B_0$ . The last term of the Hamiltonian represents the interaction between the measured magnetic field  $B_{ex}(t)$  along the x-axis and the YIG sphere, with  $\lambda = \gamma \sqrt{5N}/2$  being the corresponding interaction coefficient of external detected field-magnon.

To account for the influence of the parametric amplification interaction of magnons on the system, we diagonalize  $H_1 = \hbar\omega_0 \hat{m}^\dagger \hat{m} + \frac{\hbar\omega_m}{2} (\hat{m}^2 + \hat{m}^{\dagger 2})$  through the squeezing transformation  $\hat{m} = \cosh r_m \hat{M} + \sinh r_m \hat{M}^\dagger$ , where  $r_m = \frac{1}{4} \ln \frac{\omega_0 + \omega_m}{\omega_0 - \omega_m}$  denotes the degree of squeezing amplitude. Consequently, the Hamiltonian, after the squeezing transformation, takes the form

$$\begin{aligned} \hat{H}^s = & \hbar\omega'_a \hat{a}^\dagger \hat{a} + \hbar\omega'_0 \hat{M}^\dagger \hat{M} + \hbar g'_0 (\hat{M} + \hat{M}^\dagger) (\hat{a} + \hat{a}^\dagger) \\ & + i\hbar E_l (\hat{a}^\dagger e^{-i\omega_l t} - \hat{a} e^{i\omega_l t}) + i\hbar E_b (\hat{M}^\dagger e^{-i\omega_b t} - \hat{M} e^{i\omega_b t}) \\ & - \hbar\lambda B'_{ex}(t) (\hat{M} + \hat{M}^\dagger), \end{aligned} \quad (2)$$

where  $\omega'_0 = \omega_0 / \cosh(2r_m)$  represents the corrected magnon frequency,  $g'_0(t) = g_0(t)e^{r_m}$ , and  $B'_{ex}(t) = B_{ex}(t)e^{r_m}$  denote the enhanced cavity photon-magnon interaction intensity and the enhanced external magnetic field, respectively, and  $\omega_b$  and  $E_b$  represent the frequency and amplitude of the driving field of the magnon. Due to the external adjustable parameters  $\omega'$ ,  $\omega_l$ , and  $\omega_b$ , we set  $\omega' = \omega_l + \omega_b$  and consider the rotational wave approximation. Consequently, after rotating with the semi-classical driving field frequencies  $\omega_L$  and  $\omega_d$ , the Hamiltonian reads

$$\begin{aligned} \hat{H}' = & \hbar\Delta_a \hat{a}^\dagger \hat{a} + \hbar\Delta'_0 \hat{M}^\dagger \hat{M} + \hbar g' (\hat{M} + \hat{M}^\dagger) (\hat{a} + \hat{a}^\dagger) \\ & + i\hbar E_l (\hat{a}^\dagger - \hat{a}) + i\hbar E_b (\hat{M}^\dagger - \hat{M}) \\ & - \hbar\lambda B'_{ex}(t) (\hat{M} e^{-i\omega_b t} + \hat{M}^\dagger e^{i\omega_b t}), \end{aligned} \quad (3)$$

where  $\Delta_a = \omega_a - \omega_l$ ,  $g' = Ag_0 e^{r_m} = g e^{r_m}$ , and  $\Delta'_0 = \omega'_0 - \omega_b$  represent the detuning between the cavity field and the driving microwave field, the effective cavity magnetic coupling strength, and the detuning of the magnon relative to the magnon driving field, respectively. Notably, to meet the rotational wave approximation, we require  $g \ll \omega'$ , which can be satisfied by controlling the modulation amplitude  $A$ .

### 3. Dynamics of weak magnetic sensing system

In this section, we delve into our proposed scheme's fluctuation and dissipation dynamics. Referring to the Hamiltonian in Eq. (3) from the preceding section, we

derive the quantum Heisenberg-Langevin equation for the system [69, 70]

$$\begin{aligned}\dot{\hat{a}} &= -i\Delta_a\hat{a} - \frac{\kappa_a}{2}\hat{a} - ig'(\hat{M} + \hat{M}^\dagger) + E_l + \sqrt{\kappa_a}\hat{a}_{\text{in}}(t), \\ \dot{\hat{M}} &= -i\Delta'_0\hat{M} - \frac{\kappa_m}{2}\hat{M} - ig'(\hat{a} + \hat{a}^\dagger) + E_b + \sqrt{\kappa_m}\hat{M}_{\text{in}}(t) \\ &\quad + i\lambda B'_{ex}(t)e^{i\omega_b t},\end{aligned}\tag{4}$$

Here,  $\kappa_m$  denotes the dissipation rate of the YIG sphere, and  $\hat{a}_{\text{in}}(t)$ ,  $\hat{M}_{\text{in}}(t) = \cosh r_m \hat{m}_{\text{in}} - \sinh r_m \hat{m}_{\text{in}}^\dagger$  represent the vacuum input operator of the cavity field and the squeezed input noise operator of the magnon, respectively. The correlation functions for the input operators are given by

$$\begin{aligned}\langle \hat{a}_{\text{in}}(t)\hat{a}_{\text{in}}^\dagger(t') \rangle &= (\bar{n}_a + 1)\delta(t - t'), \\ \langle \hat{m}_{\text{in}}(t)\hat{m}_{\text{in}}^\dagger(t') \rangle &= (\bar{n}_m + 1)\delta(t - t'),\end{aligned}\tag{5}$$

where  $\bar{n}_a(\bar{n}_m) = [\exp(\hbar\omega_a(\omega_0)/k_B T) - 1]^{-1}$  represents the average number of photons (magnons) in a thermal equilibrium state [40]. The modified squeezing input operator satisfies

$$\begin{aligned}\langle \hat{M}_{\text{in}}(t)\hat{M}_{\text{in}}^\dagger(t') \rangle &= [\cosh(2r_m)\bar{n}_m + \sinh^2(r_m) + 1]\delta(t - t'), \\ \langle \hat{M}_{\text{in}}^\dagger(t)\hat{M}_{\text{in}}^\dagger(t') \rangle &= -\sinh(2r_m)(\bar{n}_m + 1/2)\delta(t - t').\end{aligned}\tag{6}$$

Since we consider a strong driving field, we can write the operator as the steady-state part plus the first-order fluctuations, i.e.,  $\hat{a}(M) = \bar{a}(\bar{m}) + \delta\hat{a}(\delta\hat{M})$ . Thus the Heisenberg-Langevin's equation can be rewritten as

$$\begin{aligned}\delta\dot{\hat{a}} &= -i\Delta_a\delta\hat{a} - \frac{\kappa_a}{2}\delta\hat{a} - ig'(\delta\hat{M} + \delta\hat{M}^\dagger) + \sqrt{\kappa_a}\hat{a}_{\text{in}}(t), \\ \delta\dot{\hat{M}} &= -i\Delta'_0\delta\hat{M} - \frac{\kappa_m}{2}\delta\hat{M} - ig'(\delta\hat{a} + \delta\hat{a}^\dagger) + \sqrt{\kappa_m}\hat{M}_{\text{in}}(t) \\ &\quad + i\lambda B'_{ex}(t)e^{i\omega_b t}.\end{aligned}\tag{7}$$

Considering the detection of the external magnetic field signal through the output of the microwave cavity field, we introduce the quadrature components  $\delta\hat{X}_a = (\hat{a}^\dagger + \hat{a})/\sqrt{2}$ ,  $\delta\hat{P}_a = (\hat{a} - \hat{a}^\dagger)/\sqrt{2}i$ ,  $\delta\hat{X}_M = (\hat{a} + \hat{a}^\dagger)/\sqrt{2}i$ ,  $\delta\hat{P}_M = (\hat{a} - \hat{a}^\dagger)/\sqrt{2}i$ . The Langevin equations for these quadrature components are

$$\begin{aligned}\delta\dot{\hat{X}}_M &= \Delta'_0\delta\hat{P}_M - \frac{\kappa_m}{2}\delta\hat{X}_M + \sqrt{\kappa_m}\hat{X}_M^{\text{in}}, \\ \delta\dot{\hat{P}}_M &= -\Delta'_0\delta\hat{X}_M - 2g'\delta\hat{X}_a - \frac{\kappa_m}{2}\delta\hat{P}_M + \sqrt{\kappa_m}\hat{P}_M^{\text{in}}, \\ \delta\dot{\hat{X}}_a &= \Delta_a\delta\hat{P}_a - \frac{\kappa_a}{2}\delta\hat{X}_a + \sqrt{\kappa_a}\hat{X}_a^{\text{in}}, \\ \delta\dot{\hat{P}}_a &= -\Delta_a\delta\hat{X}_a - 2g'\delta\hat{X}_M - \frac{\kappa_a}{2}\delta\hat{P}_a + \sqrt{\kappa_a}\hat{P}_a^{\text{in}},\end{aligned}\tag{8}$$

where  $\hat{X}_a^{\text{in}} = (\hat{a}_{\text{in}}^\dagger + \hat{a}_{\text{in}})/\sqrt{2}$ ,  $\hat{P}_a^{\text{in}} = (\hat{a}_{\text{in}} - \hat{a}_{\text{in}}^\dagger)/\sqrt{2}i$ ,  $\hat{X}_M^{\text{in}} = (\hat{M}_{\text{in}}^\dagger + \hat{M}_{\text{in}})/\sqrt{2} - \sqrt{2/\kappa_m}\lambda B'_{ex}(t)\sin(\omega_b t)$ ,  $\hat{P}_M^{\text{in}} = (\hat{M}_{\text{in}} - \hat{M}_{\text{in}}^\dagger)/\sqrt{2}i +$

$\sqrt{2/\kappa_m}\lambda B'_{ex}(t) \cos(\omega_b t) = \hat{P}_M^{\text{in}} + \sqrt{2/\kappa_m}\lambda B'_{ex}(t) \cos(\omega_b t)$  are the quadratures of the cavity field and magnon mode correction noise input operators.

According to Eqs. (6), we can find that the correlation functions for the quadratures of the magnon mode are

$$\begin{aligned} \langle \hat{X}_M^{\text{in}}(t) \hat{X}_M^{\text{in}}(t') \rangle &= e^{-2r_m} (\bar{n}_m + 1/2) \delta(t - t'), \\ \langle \hat{P}_M^{\text{in}}(t) \hat{P}_M^{\text{in}}(t') \rangle &= e^{2r_m} (\bar{n}_m + 1/2) \delta(t - t'), \end{aligned} \quad (9)$$

detailed derivation can be found in Appendix A. Eqs. (9) indicates that the magnon mode correlation function is modified to squeeze the amplitude quadrature fluctuations and increase the phase quadrature fluctuations. Therefore, we need to measure the cavity field phase quadrature to detect weak magnetic fields sensitively. Eqs. (9) indicate that the magnon mode correlation function is modified to squeeze the amplitude quadrature fluctuations and increase the phase quadrature fluctuations. Therefore, measuring the cavity field's phase quadrature is crucial for sensitively detecting weak magnetic fields. To address the impact of noise on the system, we transform Eqs. (8) into the frequency domain space using the Fourier transform  $\hat{O}(\omega) = \int_{-\infty}^{\infty} dt O(t) e^{i\omega t}$ . Utilizing the input-output relationship for the phase quadrature component  $\delta \hat{P}_a^{\text{out}} = \sqrt{\kappa_a} \delta \hat{P}_a - \hat{P}_a^{\text{in}}$ , we obtain an expression for the phase quadrature of the cavity field as

$$\begin{aligned} \delta \hat{P}_a^{\text{out}}(\omega) &= K_1(\omega) \hat{X}_m^{\text{in}}(\omega) + K_2(\omega) \hat{P}_m^{\text{in}}(\omega) + K_3(\omega) \hat{X}_a^{\text{in}}(\omega) \\ &\quad + K_4(\omega) \hat{P}_a^{\text{in}}(\omega), \end{aligned} \quad (10)$$

where

$$\begin{aligned} K_1(\omega) &= \frac{8g' \sqrt{\kappa_a \kappa_m} (\kappa_a - 2i\omega) (\kappa_m - 2i\omega)}{64\Delta'_0 \Delta_a g'^2 + [(\kappa_m - 2i\omega)^2 + 4\Delta_0'^2] (4\omega^2 + \kappa_a^2 - 4\Delta_a^2)}, \\ K_2(\omega) &= \frac{16g' \Delta'_0 \sqrt{\kappa_a \kappa_m} (\kappa_a - 2i\omega)}{64\Delta'_0 \Delta_a g'^2 + [(\kappa_m - 2i\omega)^2 + 4\Delta_0'^2] (4\omega^2 + \kappa_a^2 - 4\Delta_a^2)}, \\ K_3(\omega) &= \frac{4\kappa_a [-16g'^2 \Delta'_0 + \Delta_a [(\kappa_m - 2i\omega)^2 + 4\Delta_0'^2]]}{64\Delta'_0 \Delta_a g'^2 + [(\kappa_m - 2i\omega)^2 + 4\Delta_0'^2] (4\omega^2 + \kappa_a^2 - 4\Delta_a^2)}, \\ K_4(\omega) &= -1 - \frac{2\kappa_a (\kappa_a - 2i\omega) [(\kappa_m - 2i\omega)^2 + 4\Delta_0'^2]}{64\Delta'_0 \Delta_a g'^2 + [(\kappa_m - 2i\omega)^2 + 4\Delta_0'^2] (4\omega^2 + \kappa_a^2 - 4\Delta_a^2)}, \end{aligned} \quad (11)$$

with  $\hat{X}_M^{\text{in}}(\omega) = \hat{X}_M^{\text{in}}(\omega) + \lambda \sqrt{\frac{1}{2\kappa_m}} i [B'_{ex}(\omega + \omega_b) - B'_{ex}(\omega - \omega_b)]$  and  $\hat{P}_M^{\text{in}}(\omega) = \hat{p}_M^{\text{in}}(\omega) + \lambda \sqrt{\frac{1}{2\kappa_m}} [B'_{ex}(\omega + \omega_b) + B'_{ex}(\omega - \omega_b)]$  representing the modified quadrature component of the magnon in the frequency domain.

## 4. Weak magnetic field sensing using output spectrum analysis

### 4.1. The Role of Magnon squeezing in Anisotropic YIG Sphere

Direct homodyne detection of microwave photons remains impractical due to the experimental, developmental stage of the technology. As an alternative, microwave-to-optical frequency conversion technology offers a feasible approach by transferring

photons from the microwave to the optical frequency band [71–75]. This initial conversion step bypasses the challenges associated with direct homodyne detection of microwave photons. Subsequent optical homodyne detection, applied to the converted optical frequency photons, is considered experimentally viable. It's essential to clarify that our discussion does not delve into the specifics of conversion efficiency but emphasizes the broader implications of our proposed solution on sensing performance. Furthermore, leveraging homodyne detection, one can calculate the output spectrum of a weak magnetic field sensing system [76] as

$$S_{\text{out}}(\omega) = \frac{1}{4\pi} \int d\omega' e^{i(\omega+\omega')t} [C_P(\omega, \omega') + C_P(\omega', \omega)] \quad (12)$$

with  $C_P(\omega, \omega') = \langle \delta \hat{P}_a^{\text{out}}(\omega) \delta \hat{P}_a^{\text{out}}(\omega') \rangle$ . For the current system, we have

$$\begin{aligned} S_{\text{out}}(\omega) &= (\bar{n}_a + \frac{1}{2}) [ |K_3(\omega)|^2 + |K_4(\omega)|^2 ] \\ &\quad + |K_1(\omega)|^2 [ (\bar{n}_m + \frac{1}{2}) / \xi + S'_{B_{ex1}} ] \\ &\quad + |K_2(\omega)|^2 [ (\bar{n}_m + \frac{1}{2}) \xi + S'_{B_{ex2}} ], \end{aligned} \quad (13)$$

Where  $S'_{B_{ex1}} = \xi S_{B_{ex1}}$  and  $S'_{B_{ex2}} = \xi S_{B_{ex2}}$  are the amplified signal spectral densities of the external magnetic field corresponding to the two channels of magnon amplitude quadrature component and a phase quadrature component, respectively, with  $\xi = e^{2r_m}$  being the coefficient of amplification, from the output spectrum  $S_{\text{out}}(\omega)$ , it can be seen that the second and third terms correspond to the squeezing effect and the anti-squeezing effect of the noise, respectively. In the squeezing effect, thermal noise can be reduced, while in the anti-squeezing effect, thermal noise is amplified. Therefore, to suppress the thermal noise of the system, a prerequisite is to make  $|K_2(\omega)|^2 = 0$  so that the thermal noise only retains the squeezing effect, which can be attained by adjusting the detuning as  $\Delta_a = \Delta'_0 = 0$ . Thus, one can obtain an output spectrum as

$$S_{\text{out}}(\omega) = \frac{2\bar{n}_a + 1}{2} |K_4(\omega)|^2 + |K_1(\omega)|^2 \left[ \frac{2\bar{n}_m + 1}{2\xi} + S'_{B_{ex1}} \right]. \quad (14)$$

Eq. (14) indicates that not only the thermal fluctuations of the magnon are exponentially suppressed, but also the backaction noise of the cavity field is eliminated. This can be further understood by rewriting the Langevin equations as

$$\begin{aligned} \delta \dot{\hat{X}}_M &= -\frac{\kappa_m}{2} \delta \hat{X}_M + \sqrt{\kappa_m} \hat{X}_M^{\text{in}}, \\ \delta \dot{\hat{P}}_M &= -2g' \delta \hat{X}_a - \frac{\kappa_m}{2} \delta \hat{P}_M + \sqrt{\kappa_m} \hat{P}_M^{\text{in}}, \\ \delta \dot{\hat{X}}_a &= -\frac{\kappa_a}{2} \delta \hat{X}_a + \sqrt{\kappa_a} \hat{X}_a^{\text{in}}, \\ \delta \dot{\hat{P}}_a &= -2g' \delta \hat{X}_M - \frac{\kappa_a}{2} \delta \hat{P}_a + \sqrt{\kappa_a} \hat{P}_a^{\text{in}}. \end{aligned} \quad (15)$$

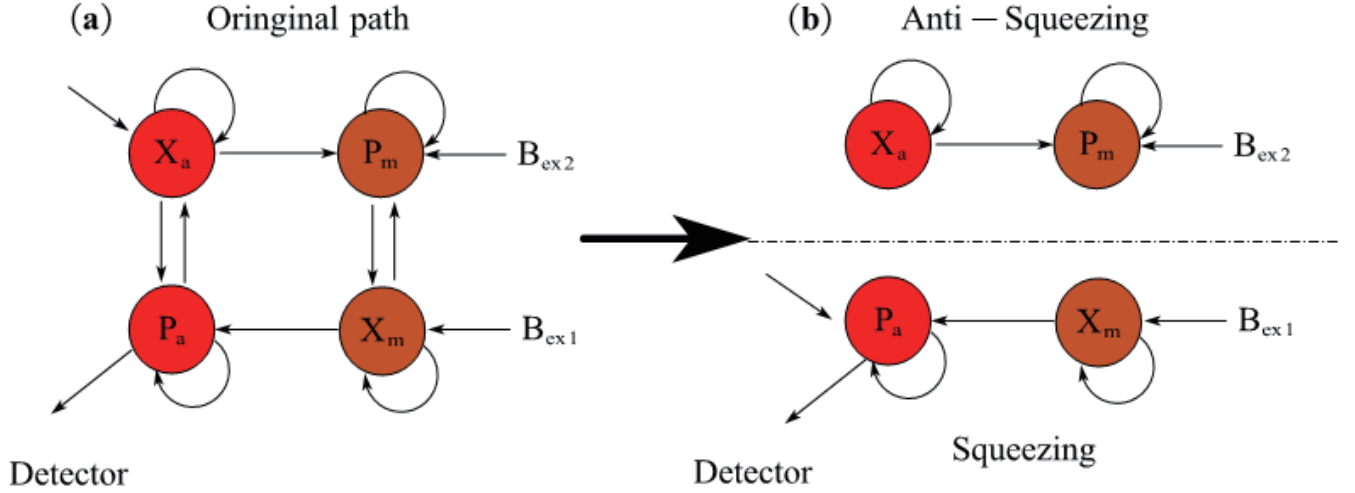


**Figure 2.** The schematic diagram of signal/noise transmission path. (a) The original path. (b) the path after implementing backaction avoidance and magnon squeezing.

It can be found that in the quadrature equations of the magnon mode (see the first two equations in Eqs. (15)), the amplitude quadrature and the phase quadrature are independent of each other. That is, the amplitude quadrature and the phase quadrature component can be measured independently simultaneously, and the phase quadrature component of the cavity field is only related to the amplitude quadrature. Therefore, our phase quadrature output spectrum will avoid the backaction noise caused by the cavity-magnon coupling effect. This is evident from the transition shown in Fig. 2, from panel (a) to panel (b). The phase quadrature component of the cavity field we aim to detect is separated into a squeezing path, enabling us to achieve low-noise sensing. On the contrary, the noise on the anti-squeezing path is amplified and captured by amplitude quadrature.

To better understand the noise suppression, one can express the output spectrum as

$$S_{\text{out}}(\omega) = A_m(\omega)[N_{\text{mth}}(\omega) + N_{\text{qn}}(\omega) + S_{B_{\text{ex1}}}], \quad (16)$$

where  $A_m(\omega)$ ,  $N_{\text{qn}}(\omega)$ , and  $N_{\text{mth}}(\omega)$  represent the system's response, additional noise, and magnon thermal noise, respectively. These are explicitly defined as

$$A_m(\omega) = \xi |K_1(\omega)|^2, \quad (17)$$

$$N_{\text{qn}}(\omega) = \frac{(\bar{n}_a + \frac{1}{2}) |K_4(\omega)|^2}{\xi |K_1(\omega)|^2}, \quad (18)$$

$$N_{\text{mth}}(\omega) = \frac{(\bar{n}_m + \frac{1}{2})}{\xi^2}. \quad (19)$$

From Eq. (17, 18, 19), we can surprisingly find that due to the squeezing effect, the response of the system to the external magnetic field can be amplified, which is conducive



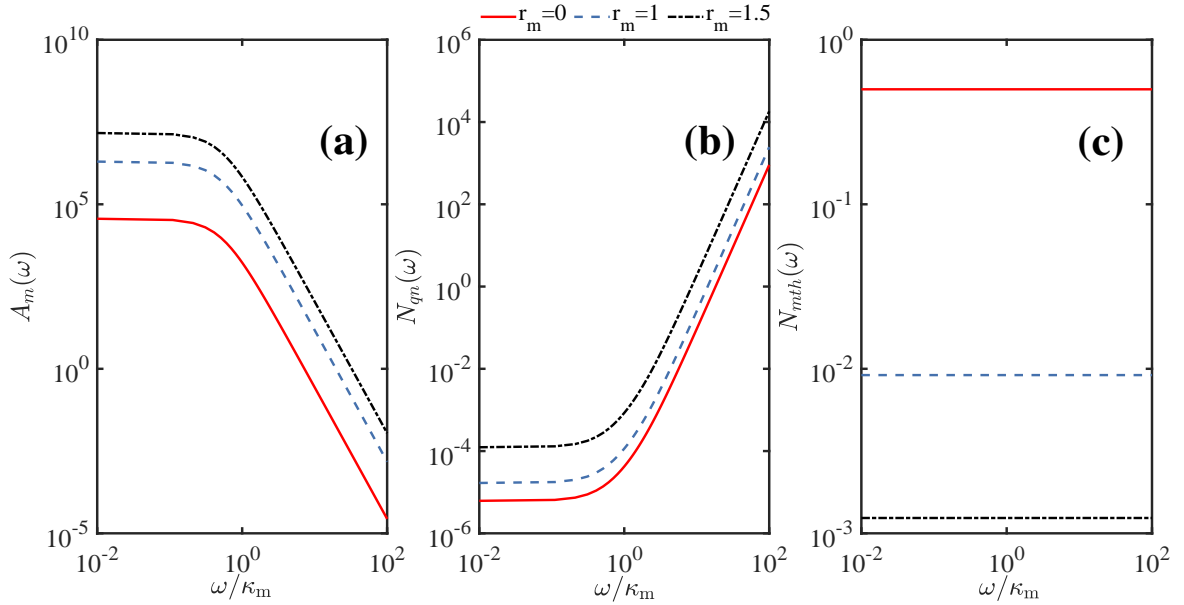


**Figure 3.** (a) The response  $A_m(\omega)$  of a weak magnetic field sensing system versus the normalized frequency  $\omega/\kappa_m$  under different squeezing parameters. (b) Additional noise  $N_{qn}(\omega)$  versus the normalized frequency  $\omega/\kappa_m$  under different squeezing parameters. (c) Thermal noise versus the normalized frequency  $\omega/\kappa_m$  under different squeezing parameters. Here, the initial environmental temperature is 50 mK. It is worth noting that the legends for Fig. (a), (b), and Fig. (c) are consistent.

to more significant sensing of extremely weak magnetic field signals. Moreover, the system's additional noise and the magnon's thermal noise are also reduced, and the thermal noise decays faster.

To elucidate the effects of various mechanisms on noise suppression, we conduct numerical simulations on several sensing performance indicators at low temperatures (50 mK), employing the experimental parameters cited in [10, 21, 66]:  $\omega_0/2\pi = \omega_a/2\pi = 37.5$  GHz,  $\lambda/2\pi = 14 \times \sqrt{17.5}$  THz,  $g/2\pi = 2.5$  GHz,  $\kappa_m/2\pi = 15$  MHz, and  $\kappa_a/2\pi = 16.5$  MHz. Fig. 2(a) illustrates the response of the weak magnetic field sensing system. As the squeezing parameters increase, the signal amplification effect strengthens, attributed to the parametric amplification interaction of magnons acting as a parametric amplifier, thereby enhancing the external signal. Figs. 3(b) and 3(c) depict the suppression effect of magnon squeezing on additional noise and thermal noise, respectively. With increasing squeezing parameters, thermal and additional noise decrease by approximately three orders of magnitude. This reduction is straightforwardly understood as magnon squeezing significantly reduces vacuum fluctuations, leading to observable thermal noise decay. Additionally, the effective amplification of the signal through magnon squeezing results in a noticeable reduction of additional noise. This phenomenon is clearly illustrated in the comparison between Fig. 3(a) and 3(b). Furthermore, to evaluate the impact of cavity field dissipation on the sensing performance of the system, we plotted the variation curves of response,

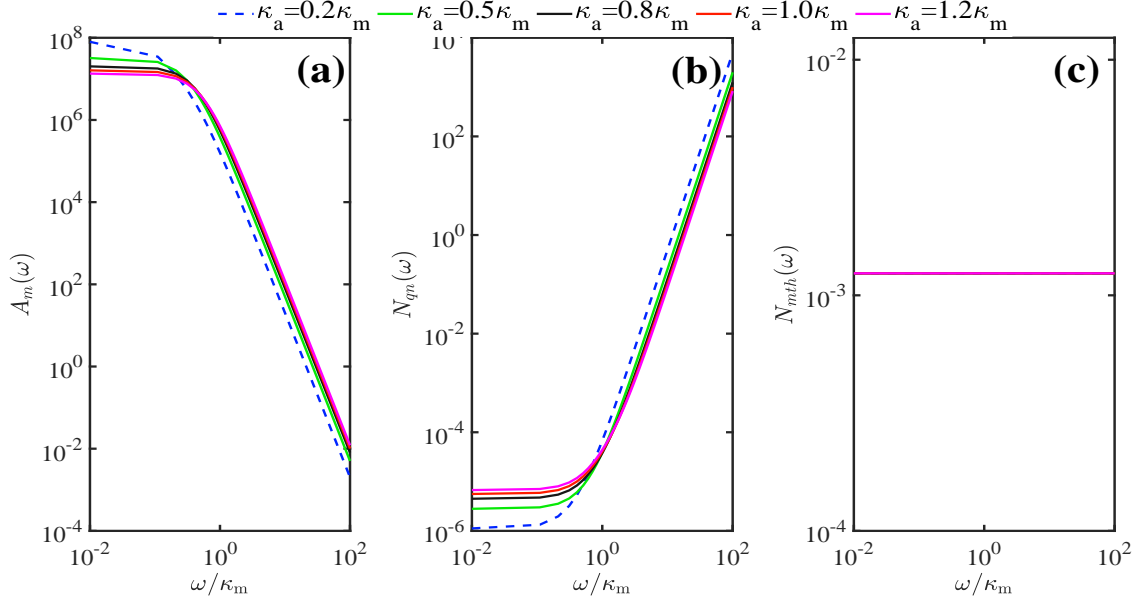


**Figure 4.** (a) The response  $A_m(\omega)$  of a weak magnetic field sensing system versus the normalized frequency  $\omega/\kappa_m$  under different cavity field dissipation. (b) Additional noise  $N_{qn}(\omega)$  versus the normalized frequency  $\omega/\kappa_m$  under different cavity field dissipation. (c) Thermal noise versus the normalized frequency  $\omega/\kappa_m$  under different cavity field dissipation. The initial environmental temperature is 50 mK, squeezing parameter  $r_m = 1.5$ . It is worth noting that the legends for Fig. (a), (b), and Fig. (c) are consistent.

additional noise, and thermal noise at different cavity field dissipation rates, as illustrated in Fig. 4. The results indicate that increased cavity field dissipation adversely affects both the response and additional noise metrics (Fig. 5(a), (b)). This is because dissipation heightens the quantum noise within the cavity field, diminishing its ability to respond to the original signal accurately. Conversely, thermal noise remains unaffected by changes in cavity field dissipation, as depicted in Fig. 5(c). This is because thermal noise, having been normalized, is essentially background noise influenced solely by squeezing parameters. Another parameter that significantly influences the response and additional noise is the cavity-magnon coupling strength, as depicted in Fig. 5(a) and Fig. 5(b). As the coupling strength increases, the response is enhanced, resulting in an amplified signal of the external magnetic field and a corresponding suppression of additional noise. This phenomenon can be explained from a physical perspective; with an increase in the cavity magnetic coupling strength, the energy exchange between the cavity photon-major systems becomes more efficient, facilitating the extraction of information regarding the external magnetic field.

To perform a detailed analysis of the system's sensitivity, we consider the total noise spectral density of the system. According to Eq. (10), the total noise amplitude can be expressed as

$$\hat{B}_{noise}(\omega) = \frac{\sqrt{2\kappa_m}}{\lambda\xi} \hat{X}_m^{\text{in}}(\omega) + \frac{\sqrt{2\kappa_m}K_4(\omega)}{K_1(\omega)\lambda\sqrt{\xi}} \hat{P}_a^{\text{in}}(\omega). \quad (20)$$

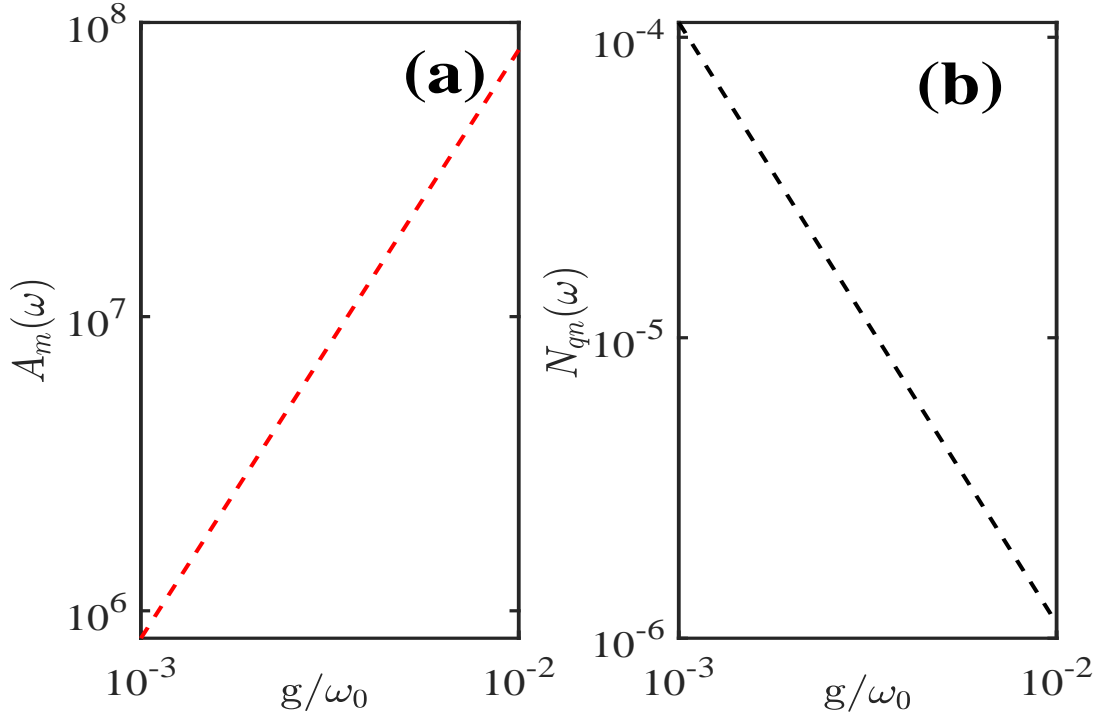


**Figure 5.** (a) The response  $A_m(\omega)$  of a weak magnetic field sensing system versus the normalized frequency  $\omega/\kappa_m$  under different cavity- magnon coupling strengths. (b) Additional noise  $N_{qn}(\omega)$  versus the normalized frequency  $\omega/\kappa_m$  under different cavity-magnon coupling strengths. Here, the initial environmental temperature is 50 mK, squeezing parameter  $r_m = 1.5$ ,  $\kappa_a = 0.2\kappa_m$ .

The total noise intensity can be quantified using the symmetric noise power spectral density. This measure is directly detectable by a quantum spectrum analyzer and is defined as follows [59]

$$S_{Bnoise}(\omega)\delta(\omega + \omega') = \frac{1}{2}(\langle \hat{B}_{noise}(\omega)\hat{B}_{noise}(\omega') \rangle + c.c.). \quad (21)$$

Thus, the total noise spectrum can be given as

$$S_{Bnoise}(\omega) = \frac{2\kappa_m}{\lambda^2}[N_{Mth}(\omega) + N_{ad}(\omega)]. \quad (22)$$

Next, we further discuss the system's signal-to-noise ratio to define its sensitivity. Generally speaking, the signal-to-noise ratio is the ratio of the measured signal to noise. For our system, it can be written in the following form

$$B_{SNR}(\omega) = \frac{|B_{ex}(\omega)|}{\sqrt{S_{Bnoise}(\omega)}}, \quad (23)$$

the numerator represents the signal of the external magnetic field to be measured, and the denominator represents the noise information. To find the minimum detectable signal, we set the signal-to-noise ratio to 1, which can provide the minimum detectable

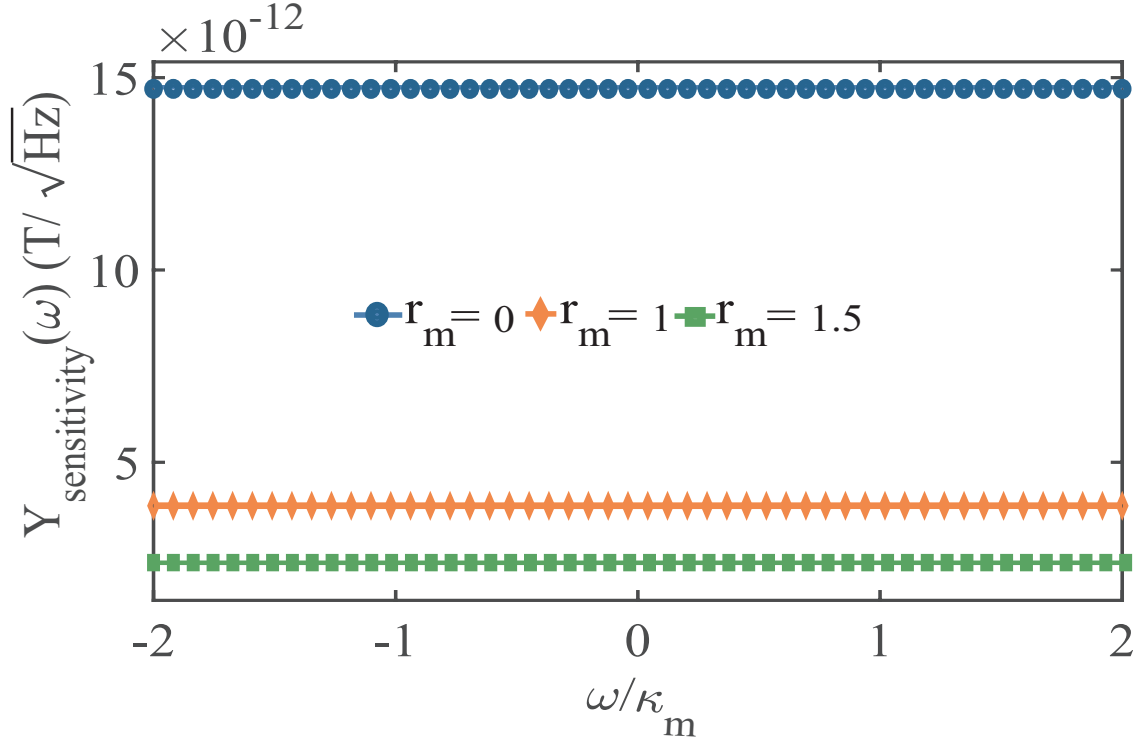


**Figure 6.** The sensitivity  $Y_{\text{sensitivity}}(\omega)$  of a weak magnetic field sensing system versus the normalized frequency  $\omega/\kappa_m$  under different squeezing parameters. We set the initial environmental temperature to be 280 K.

signal, i.e.,  $B_{\text{dmin}} = \sqrt{S_{\text{Bnoise}}(\omega)}$  can be given. Therefore, we define the minimum detectable signal as sensitivity [10, 76], which is defined as

$$\begin{aligned} Y_{\text{sensitivity}}(\omega) &= \sqrt{S_{\text{Bnoise}}(\omega)} \\ &= \frac{\sqrt{2\kappa_m[N_{\text{Mth}}(\omega) + N_{\text{ad}}(\omega)]}}{\lambda}. \end{aligned} \quad (24)$$

The sensitivity of the system depends on the additional noise and magnon thermal noise, the dissipation rate ( $\kappa_m$ ) of the YIG sphere, and the coupling strength ( $\lambda$ ) of the external magnetic field. A smaller  $Y_{\text{sensitivity}}(\omega)$  value indicates higher sensitivity.

In Fig. 6, we plot the sensitivity of the weak magnetic sensing system as a function of the normalized frequency  $\omega/\kappa_m$  under different squeezing parameters. At room temperature, our sensitivity improves by one order of magnitude compared to without magnon squeezing. Furthermore, we observe that the sensitivity remains relatively constant with the normalized frequency, indicating that thermal noise predominantly influences the system. Nonetheless, our results demonstrate a significant enhancement over the scenario without squeezing.

#### 4.2. The Role of Magnon Squeezed Vacuum Reservoir

In this section, we demonstrate that introducing a specific magnon-squeezed vacuum reservoir for continued suppression of thermal noise can significantly enhance sensitive

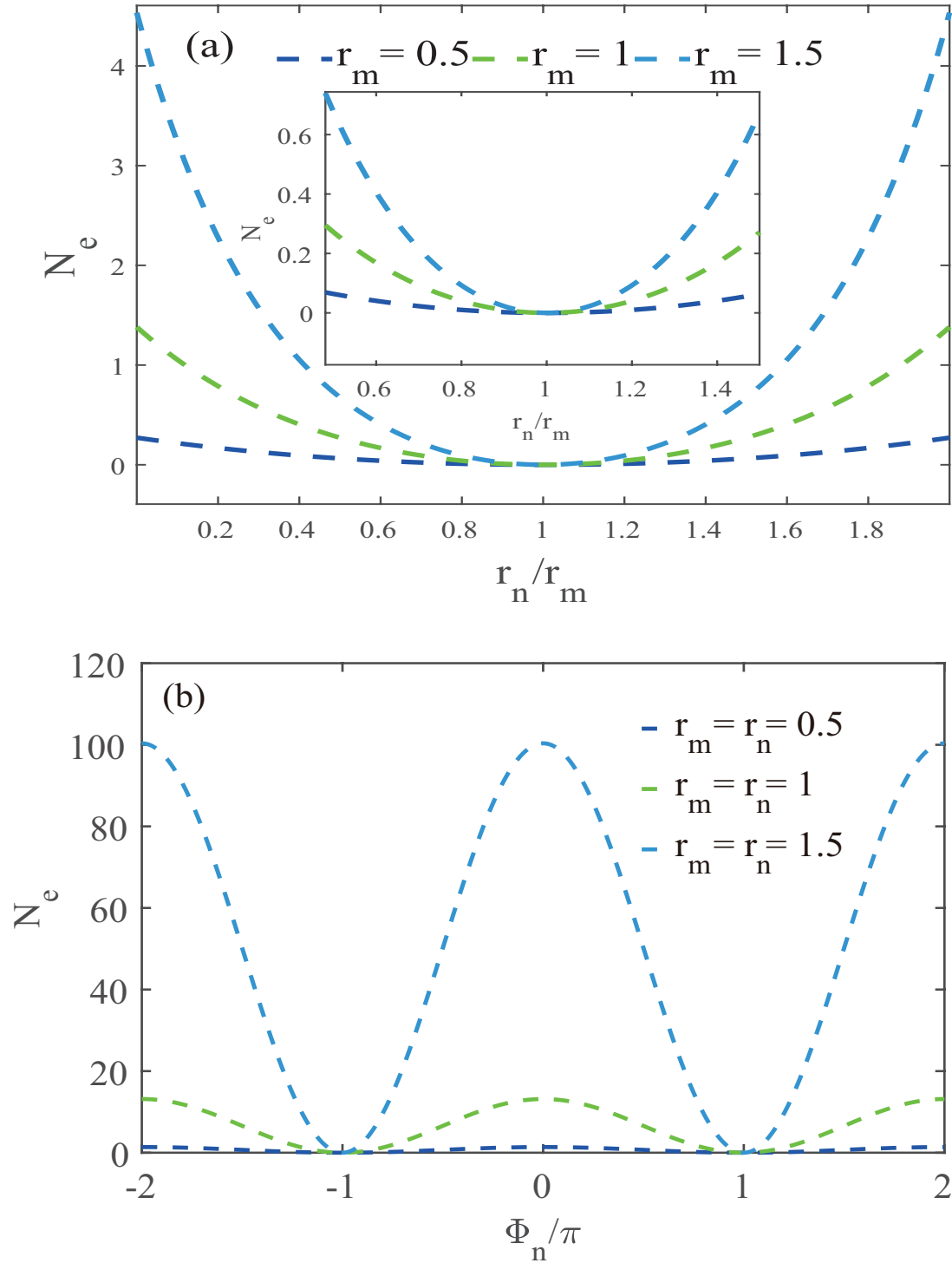


**Figure 7.** (a) The corrected effective average number of magnon  $N_e$  versus the relative squeezing parameters  $r_n/r_m$ . (b) The corrected effective average number of magnon  $N_e$  versus the squeezing phase  $\Phi_n/\pi$ .

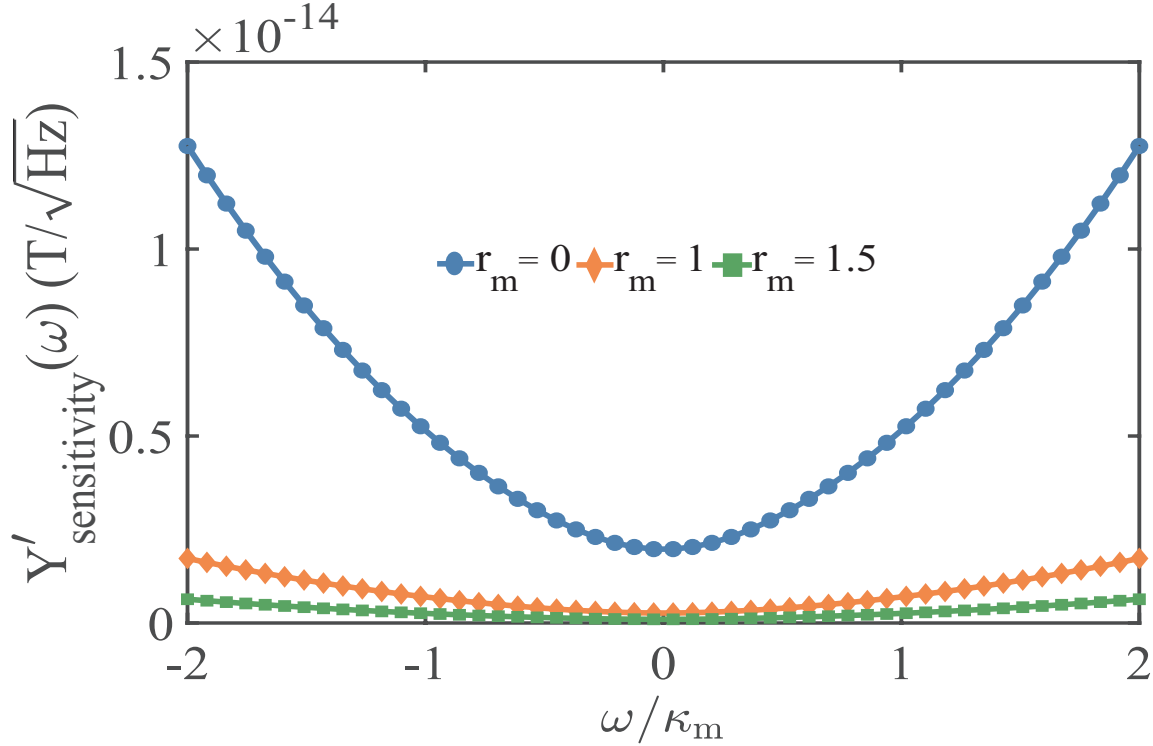


**Figure 8.** The sensitivity  $Y'_{\text{sensitivity}}(\omega)$  versus the normalized frequency  $\omega/\kappa_m$  under different squeezing parameters. We set the initial environmental temperature to be 280 K.

sensing performance. We introduce a magnon squeezing vacuum reservoir with a squeezing parameter  $r_n$  and a phase  $\Phi_n$ . Consequently, the correlation function of the input noise operator of the magnon can be further modified as follows

$$\begin{aligned}
 \langle M_{in}^c(t)M_{in}^{c\dagger}(t') \rangle &= (N_e + 1) \delta(t - t'), \\
 \langle M_{in}^{c\dagger}(t)M_{in}^c(t') \rangle &= N_e \delta(t - t'), \\
 \langle M_{in}^{c\dagger}(t)M_{in}^{c\dagger}(t') \rangle &= M_e \delta(t - t'), \\
 \langle M_{in}^{c\dagger}(t)M_{in}^{c\dagger}(t') \rangle &= M_e^* \delta(t - t').
 \end{aligned} \tag{25}$$

where

$$\begin{aligned}
 N_e &= \sinh^2(r_n) \cosh^2(r_m) + \sinh^2(r_m) \cosh^2(r_n) + \\
 &\quad \frac{1}{2} \cos(\Phi_n) \sinh(2r_n) \sinh(2r_m), \\
 M_e &= [\cosh(r_n) \sinh(r_m) + e^{i\Phi_n} \sinh(r_n) \cosh(r_m)] \times \\
 &\quad [\cosh(r_n) \cosh(r_m) + e^{-i\Phi_n} \sinh(r_n) \sinh(r_m)],
 \end{aligned} \tag{26}$$

represent the corrected effective average number of magnons and the interaction coefficient of two magnons, respectively [77]. In Fig. 7, we plot the curve of  $N_e$  as

a function of the squeezing parameter and phase of the vacuum reservoir. Notably, if  $r_n = r_m$  and  $\Phi = \pm\pi$ , the effective number of magnons reduces to zero, leading to a simplified expression of sensitivity

$$Y'_{sensitivity}(\omega) \approx \frac{\sqrt{2\kappa_m N_{ad}(\omega)}}{\lambda}. \quad (27)$$

This implies complete suppression of magnon thermal noise, with sensitivity  $Y'_{sensitivity}$  solely dependent on the additional noise  $N_{ad}$  of the weak magnetic field sensing system, a component of the microwave cavity field. Furthermore, given the previous achievement of backaction evading, the sensing system's noise is only part of the shot noise of the cavity field. To better highlight the significant advantage of combining the parametric amplification effect of squeezed vacuum reservoirs and magnons on sensitivity, as shown in Fig. 8, we plot the sensitivity with different squeezing parameters under complete suppression of magnon thermal noise. Surprisingly, with a squeezing parameter  $r_m = 1.5$ , the sensitivity reaches the  $\text{fT}/\sqrt{\text{Hz}}$  level at room temperature (280K). Therefore, our theoretical scheme can achieve ultra-high sensitivity weak magnetic field sensing.

## 5. DISCUSSION and CONCLUSIONS

In this paper, we achieved magnon squeezing interaction through an anisotropic YIG sphere. Additionally, squeezing may be induced by various methods such as utilizing squeezed vacuum fields [78], employing dual-tone microwave fields to stimulate magnon mode [79], or utilizing two microwave fields to drive qubits within a magnetic qubit system nested in a cavity [80]. Our study focuses on suppressing thermal noise in weak magnetic sensing within cavity magnon systems. We propose modifying the shape of the YIG sphere from spherical to ellipsoidal to achieve magnon squeezing and alter the correlation function of the quadrature components of the magnon mode, resulting in significant suppression of thermal noise. Furthermore, successfully coupling the YIG sphere magnon with a squeezed vacuum reservoir can enable perfect thermal noise suppression, allowing the system sensitivity to reach the order of  $\text{fT}$  even at room temperature. Our scheme provides a crucial foundation for improvement in weak magnetic field sensing. Magnons serve as excellent probes for external magnetic fields, and achieving low noise in microwave cavities and ultrastrong coupling of cavity photon-magnon facilitates converting the external magnetic field signal through magnons to photons, detectable by spectral analyzers. Moreover, in dark matter detection, the coupling between axions and standard model matter can generate a pseudo magnetic field detectable by magnons, with the extracted signal detectable by the optical readout, as initially proposed in [81]. The idea and experimentation of using cavity magnetic systems for weak magnetic field sensing have been continually evolving [82–85], providing a promising platform for dark matter detection. Although experimentally realizing a squeezed vacuum reservoir for magnons remains challenging, there is relevant literature on preparing single-mode and dual-mode squeezed states of magnons [86–89]. This can

be achieved through other methods, such as reservoir engineering or optical lattice. Moving forward, we aim to investigate the impact of entanglement and other quantum resources on weak magnetic field sensing.

## Appendix A. Modified Magnon Correlation Functions

In this section, we derive the correlation function for the quadrature components of the magnon mode, as presented in Eqs. (9) in the main text.

For a magnon mode located in a thermal equilibrium reservoir, its input correlation function is expressed in the following form

$$\begin{aligned}\langle \hat{m}_{\text{in}}(t)\hat{m}_{\text{in}}^\dagger(t') \rangle &= (\bar{n}_m + 1)\delta(t - t'), \\ \langle \hat{m}_{\text{in}}^\dagger(t)\hat{m}_{\text{in}}(t') \rangle &= \bar{n}_m\delta(t - t'),\end{aligned}\tag{A.1}$$

In the main text, we introduce the correlation function satisfied by the input noise operator after squeezing transformation  $\hat{m} = \cosh r_m \hat{M} + \sinh r_m \hat{M}^\dagger$  as follows

$$\begin{aligned}\langle \hat{M}_{\text{in}}(t)\hat{M}_{\text{in}}^\dagger(t') \rangle &= [\cosh(2r_m)\bar{n}_m + \sinh^2(r_m) + 1]\delta(t - t'), \\ \langle \hat{M}_{\text{in}}^\dagger(t)\hat{M}_{\text{in}}^\dagger(t') \rangle &= -\sinh(2r_m)(\bar{n}_m + 1/2)\delta(t - t'), \\ \langle \hat{M}_{\text{in}}(t)\hat{M}_{\text{in}}(t') \rangle &= -\sinh(2r_m)(\bar{n}_m + 1/2)\delta(t - t'), \\ \langle \hat{M}_{\text{in}}^\dagger(t)\hat{M}_{\text{in}}(t') \rangle &= [\cosh(2r_m)\bar{n}_m + \sinh^2(r_m)]\delta(t - t').\end{aligned}\tag{A.2}$$

Next, we introduce the quadrature components of the amplitude and phase of the magnon mode, which are expressed as follows

$$\begin{aligned}\hat{X}_M^{\text{in}} &= (\hat{M}_{\text{in}}^\dagger + \hat{M}_{\text{in}})/\sqrt{2}, \\ \hat{P}_M^{\text{in}} &= (\hat{M}_{\text{in}} - \hat{M}_{\text{in}}^\dagger)/\sqrt{2}i.\end{aligned}\tag{A.3}$$

Afterwards, we calculate the two relationships of Eqs. (9), The correlation functions for amplitude and phase quadrature components of magnon mode are

$$\begin{aligned}\langle \hat{X}_M^{\text{in}}(t)\hat{X}_M^{\text{in}}(t') \rangle &= \frac{1}{2} \left[ \langle \hat{M}_{\text{in}}(t)\hat{M}_{\text{in}}(t') \rangle + \langle \hat{M}_{\text{in}}(t)\hat{M}_{\text{in}}^\dagger(t') \rangle + \langle \hat{M}_{\text{in}}^\dagger(t)\hat{M}_{\text{in}}(t') \rangle + \langle \hat{M}_{\text{in}}^\dagger(t)\hat{M}_{\text{in}}^\dagger(t') \rangle \right] \\ &= \frac{1}{2} [-2\sinh(2r_m)(\bar{n}_m + 1/2) + 2\cosh(2r_m)\bar{n}_m + 2\sinh^2(r_m) + 1] \\ &= \frac{1}{2} [-2\sinh(2r_m)(\bar{n}_m + 1/2) + 2\cosh(2r_m)\bar{n}_m + \cosh(2r_m)] \\ &= \frac{1}{2} [-2\sinh(2r_m)(\bar{n}_m + 1/2) + 2\cosh(2r_m)(\bar{n}_m + 1/2)] \\ &= e^{-2r_m}(\bar{n}_m + 1/2)\delta(t - t').\end{aligned}\tag{A.4}$$



$$\begin{aligned}
\langle \hat{P}_M^{\text{in}}(t) \hat{P}_M^{\text{in}}(t') \rangle &= -\frac{1}{2} \left[ \langle \hat{M}_{\text{in}}(t) \hat{M}_{\text{in}}(t') \rangle - \langle \hat{M}_{\text{in}}(t) \hat{M}_{\text{in}}^\dagger(t') \rangle - \langle \hat{M}_{\text{in}}^\dagger(t) \hat{M}_{\text{in}}(t') \rangle + \langle \hat{M}_{\text{in}}^\dagger(t) \hat{M}_{\text{in}}^\dagger(t') \rangle \right] \\
&= -\frac{1}{2} \left[ -2 \sinh(2r_m)(\bar{n}_m + 1/2) - 2 \cosh(2r_m)\bar{n}_m - 2 \sinh^2(r_m) - 1 \right] \\
&= -\frac{1}{2} \left[ -2 \sinh(2r_m)(\bar{n}_m + 1/2) - 2 \cosh(2r_m)\bar{n}_m - \cosh(2r_m) \right] \\
&= -\frac{1}{2} \left[ -2 \sinh(2r_m)(\bar{n}_m + 1/2) - 2 \cosh(2r_m)(\bar{n}_m + 1/2) \right] \\
&= e^{2r_m}(\bar{n}_m + 1/2)\delta(t - t'). \tag{A.5}
\end{aligned}$$

So, we obtained Eqs. (9) in the main text.

## Acknowledgments

This work was supported by the National Natural Science Foundation of China under Grants Nos. 12175029, 12011530014, and 11775040 and the Key Research and Development Project of Liaoning Province under Grant No. 2020JH2/10500003.

## Disclosures

The authors declare no conflicts of interest related to this article.

## References

- [1] Degen C L, Reinhard F and Cappellaro P 2017 *Rev. Mod. Phys.* **89**(3) 035002 URL <https://link.aps.org/doi/10.1103/RevModPhys.89.035002>
- [2] Forstner S, Prams S, Knittel J, van Ooijen E D, Swaim J D, Harris G I, Szorkovszky A, Bowen W P and Rubinsztein-Dunlop H 2012 *Phys. Rev. Lett.* **108**(12) 120801 URL <https://link.aps.org/doi/10.1103/PhysRevLett.108.120801>
- [3] Takeuchi Y, Matsuzaki Y, Miyanishi K, Sugiyama T and Munro W J 2019 *Phys. Rev. A* **99**(2) 022325 URL <https://link.aps.org/doi/10.1103/PhysRevA.99.022325>
- [4] Long X, He W T, Zhang N N, Tang K, Lin Z, Liu H, Nie X, Feng G, Li J, Xin T, Ai Q and Lu D 2022 *Phys. Rev. Lett.* **129**(7) 070502 URL <https://link.aps.org/doi/10.1103/PhysRevLett.129.070502>
- [5] Kumar P, Biswas T, Feliz K, Kanamoto R, Chang M S, Jha A K and Bhattacharya M 2021 *Phys. Rev. Lett.* **127**(11) 113601 URL <https://link.aps.org/doi/10.1103/PhysRevLett.127.113601>
- [6] Li B B, Bilek J, Hoff U B, Madsen L S, Forstner S, Prakash V, Schäfermeier C, Gehring T, Bowen W P and Andersen U L 2018 *Optica* **5** 850–856 URL <https://opg.optica.org/optica/abstract.cfm?URI=optica-5-7-850>
- [7] Forstner S, Sheridan E, Knittel J, Humphreys C L, Brawley G A, Rubinsztein-Dunlop H and Bowen W P 2014 *Advanced Materials* **26** 6348–6353 URL <https://onlinelibrary.wiley.com/doi/abs/10.1002/adma.201401144>
- [8] Barry J F, Irion R A, Steinecker M H, Freeman D K, Kedziora J J, Wilcox R G and Braje D A 2023 *Phys. Rev. Appl.* **19**(4) 044044 URL <https://link.aps.org/doi/10.1103/PhysRevApplied.19.044044>
- [9] Cao Y and Yan P 2019 *Phys. Rev. B* **99**(21) 214415 URL <https://link.aps.org/doi/10.1103/PhysRevB.99.214415>

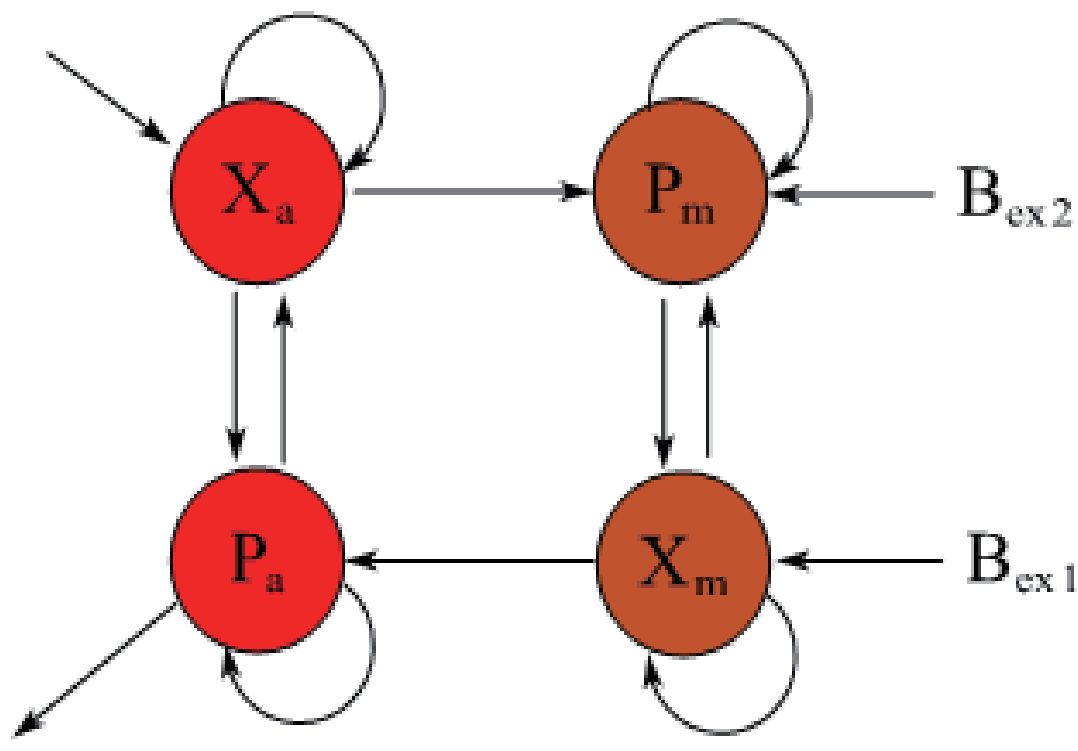
- [10] Ebrahimi M S, Motazedifard A and Harouni M B 2021 *Phys. Rev. A* **103**(6) 062605 URL <https://link.aps.org/doi/10.1103/PhysRevA.103.062605>
- [11] Xu A N and Liu Y C 2022 *Phys. Rev. A* **106**(1) 013506 URL <https://link.aps.org/doi/10.1103/PhysRevA.106.013506>
- [12] Schliesser A, Anetsberger G, Rivière R, Arcizet O and Kippenberg T J 2008 *New Journal of Physics* **10** 095015 URL <https://dx.doi.org/10.1088/1367-2630/10/9/095015>
- [13] Anetsberger G, Gavartin E, Arcizet O, Unterreithmeier Q P, Weig E M, Gorodetsky M L, Kotthaus J P and Kippenberg T J 2010 *Phys. Rev. A* **82**(6) 061804 URL <https://link.aps.org/doi/10.1103/PhysRevA.82.061804>
- [14] Li B B, Bulla D, Prakash V, Forstner S, Dehghan-Manshadi A, Rubinsztein-Dunlop H, Foster S and Bowen W P 2018 *APL Photonics* **3** 120806 ISSN 2378-0967 URL <https://doi.org/10.1063/1.5055029>
- [15] Colombano M F, Arregui G, Bonell F, Capuj N E, Chavez-Angel E, Pitanti A, Valenzuela S O, Sotomayor-Torres C M, Navarro-Urrios D and Costache M V 2020 *Phys. Rev. Lett.* **125**(14) 147201 URL <https://link.aps.org/doi/10.1103/PhysRevLett.125.147201>
- [16] Chu P H, Kim Y J and Savukov I 2019 *Phys. Rev. D* **99**(7) 075031 URL <https://link.aps.org/doi/10.1103/PhysRevD.99.075031>
- [17] Clerk A A, Devoret M H, Girvin S M, Marquardt F and Schoelkopf R J 2010 *Rev. Mod. Phys.* **82**(2) 1155–1208 URL <https://link.aps.org/doi/10.1103/RevModPhys.82.1155>
- [18] Safavi-Naeini A H, Chan J, Hill J T, Gröblacher S, Miao H, Chen Y, Aspelmeyer M and Painter O 2013 *New Journal of Physics* **15** 035007 URL <https://dx.doi.org/10.1088/1367-2630/15/3/035007>
- [19] Zhang W Z, Chen L B, Cheng J and Jiang Y F 2019 *Phys. Rev. A* **99**(6) 063811 URL <https://link.aps.org/doi/10.1103/PhysRevA.99.063811>
- [20] Rao J, Wang C Y, Yao B, Chen Z J, Zhao K X and Lu W 2023 *Phys. Rev. Lett.* **131**(10) 106702 URL <https://link.aps.org/doi/10.1103/PhysRevLett.131.106702>
- [21] Zhang X, Zou C L, Jiang L and Tang H X 2014 *Phys. Rev. Lett.* **113**(15) 156401 URL <https://link.aps.org/doi/10.1103/PhysRevLett.113.156401>
- [22] Zare Rameshti B, Viola Kusminskiy S, Haigh J A, Usami K, Lachance-Quirion D, Nakamura Y, Hu C M, Tang H X, Bauer G E and Blanter Y M 2022 *Physics Reports* **979** 1–61 ISSN 0370-1573 cavity Magnonics URL <https://www.sciencedirect.com/science/article/pii/S0370157322002460>
- [23] Zhang X, Zou C L, Jiang L and Tang H X 2016 *Science Advances* **2** e1501286 URL <https://www.science.org/doi/abs/10.1126/sciadv.1501286>
- [24] Hussain B, Qamar S and Irfan M 2022 *Phys. Rev. A* **105**(6) 063704 URL <https://link.aps.org/doi/10.1103/PhysRevA.105.063704>
- [25] Sharma S, Blanter Y M and Bauer G E W 2017 *Phys. Rev. B* **96**(9) 094412 URL <https://link.aps.org/doi/10.1103/PhysRevB.96.094412>
- [26] Cherepanov V, Kolokolov I and L'vov V 1993 *Physics Reports* **229** 81–144 ISSN 0370-1573 URL <https://www.sciencedirect.com/science/article/pii/0370157393901070>
- [27] Goryachev M, Farr W G, Creedon D L, Fan Y, Kostylev M and Tobar M E 2014 *Phys. Rev. Appl.* **2**(5) 054002 URL <https://link.aps.org/doi/10.1103/PhysRevApplied.2.054002>
- [28] Bourhill J, Kostylev N, Goryachev M, Creedon D L and Tobar M E 2016 *Phys. Rev. B* **93**(14) 144420 URL <https://link.aps.org/doi/10.1103/PhysRevB.93.144420>
- [29] Kittel C 1948 *Phys. Rev.* **73**(2) 155–161 URL <https://link.aps.org/doi/10.1103/PhysRev.73.155>
- [30] Soykal O O and Flatté M E 2010 *Phys. Rev. Lett.* **104**(7) 077202 URL <https://link.aps.org/doi/10.1103/PhysRevLett.104.077202>
- [31] Haigh J A, Nunnenkamp A, Ramsay A J and Ferguson A J 2016 *Phys. Rev. Lett.* **117**(13) 133602 URL <https://link.aps.org/doi/10.1103/PhysRevLett.117.133602>
- [32] Osada A, Hisatomi R, Noguchi A, Tabuchi Y, Yamazaki R, Usami K, Sadgrove M, Yalla R, Nomura M and Nakamura Y 2016 *Phys. Rev. Lett.* **116**(22) 223601 URL

- <https://link.aps.org/doi/10.1103/PhysRevLett.116.223601>
- [33] Zhang X, Zhu N, Zou C L and Tang H X 2016 *Phys. Rev. Lett.* **117**(12) 123605 URL <https://link.aps.org/doi/10.1103/PhysRevLett.117.123605>
- [34] Viola Kusminskiy S, Tang H X and Marquardt F 2016 *Phys. Rev. A* **94**(3) 033821 URL <https://link.aps.org/doi/10.1103/PhysRevA.94.033821>
- [35] Fan Z Y, Shen R C, Wang Y P, Li J and You J Q 2022 *Phys. Rev. A* **105**(3) 033507 URL <https://link.aps.org/doi/10.1103/PhysRevA.105.033507>
- [36] Ren Y l, Ma S l and Li F l 2022 *Phys. Rev. A* **106**(5) 053714 URL <https://link.aps.org/doi/10.1103/PhysRevA.106.053714>
- [37] Wolski S P, Lachance-Quirion D, Tabuchi Y, Kono S, Noguchi A, Usami K and Nakamura Y 2020 *Phys. Rev. Lett.* **125**(11) 117701 URL <https://link.aps.org/doi/10.1103/PhysRevLett.125.117701>
- [38] Xie J k, Ma S l and Li F l 2020 *Phys. Rev. A* **101**(4) 042331 URL <https://link.aps.org/doi/10.1103/PhysRevA.101.042331>
- [39] Kim T, Leiner J C, Park K, Oh J, Sim H, Iida K, Kamazawa K and Park J G 2018 *Phys. Rev. B* **97**(20) 201113 URL <https://link.aps.org/doi/10.1103/PhysRevB.97.201113>
- [40] Li J, Zhu S Y and Agarwal G S 2018 *Phys. Rev. Lett.* **121**(20) 203601 URL <https://link.aps.org/doi/10.1103/PhysRevLett.121.203601>
- [41] Zhang Z, Scully M O and Agarwal G S 2019 *Phys. Rev. Res.* **1**(2) 023021 URL <https://link.aps.org/doi/10.1103/PhysRevResearch.1.023021>
- [42] Yuan H Y, Yan P, Zheng S, He Q Y, Xia K and Yung M H 2020 *Phys. Rev. Lett.* **124**(5) 053602 URL <https://link.aps.org/doi/10.1103/PhysRevLett.124.053602>
- [43] Sun F X, Zheng S S, Xiao Y, Gong Q, He Q and Xia K 2021 *Phys. Rev. Lett.* **127**(8) 087203 URL <https://link.aps.org/doi/10.1103/PhysRevLett.127.087203>
- [44] Xu J, Zhong C, Han X, Jin D, Jiang L and Zhang X 2020 *Phys. Rev. Lett.* **125**(23) 237201 URL <https://link.aps.org/doi/10.1103/PhysRevLett.125.237201>
- [45] Kong C, Xiong H and Wu Y 2019 *Phys. Rev. Appl.* **12**(3) 034001 URL <https://link.aps.org/doi/10.1103/PhysRevApplied.12.034001>
- [46] Wang Y P, Rao J W, Yang Y, Xu P C, Gui Y S, Yao B M, You J Q and Hu C M 2019 *Phys. Rev. Lett.* **123**(12) 127202 URL <https://link.aps.org/doi/10.1103/PhysRevLett.123.127202>
- [47] Zhu N, Han X, Zou C L, Xu M and Tang H X 2020 *Phys. Rev. A* **101**(4) 043842 URL <https://link.aps.org/doi/10.1103/PhysRevA.101.043842>
- [48] Yu T, Zhang Y X, Sharma S, Zhang X, Blanter Y M and Bauer G E W 2020 *Phys. Rev. Lett.* **124**(10) 107202 URL <https://link.aps.org/doi/10.1103/PhysRevLett.124.107202>
- [49] Ren Y l, Ma S l, Xie J k, Li X k, Cao M t and Li F l 2022 *Phys. Rev. A* **105**(1) 013711 URL <https://link.aps.org/doi/10.1103/PhysRevA.105.013711>
- [50] Harder M, Yang Y, Yao B M, Yu C H, Rao J W, Gui Y S, Stamps R L and Hu C M 2018 *Phys. Rev. Lett.* **121**(13) 137203 URL <https://link.aps.org/doi/10.1103/PhysRevLett.121.137203>
- [51] Xu P C, Rao J W, Gui Y S, Jin X and Hu C M 2019 *Phys. Rev. B* **100**(9) 094415 URL <https://link.aps.org/doi/10.1103/PhysRevB.100.094415>
- [52] Yang Y, Wang Y P, Rao J W, Gui Y S, Yao B M, Lu W and Hu C M 2020 *Phys. Rev. Lett.* **125**(14) 147202 URL <https://link.aps.org/doi/10.1103/PhysRevLett.125.147202>
- [53] Lu T X, Zhang H, Zhang Q and Jing H 2021 *Phys. Rev. A* **103**(6) 063708 URL <https://link.aps.org/doi/10.1103/PhysRevA.103.063708>
- [54] Liu Z, Liu Y q, Mai Z y, Yang Y j, Zhou N n and Yu C s 2024 *Phys. Rev. A* **109**(2) 023709 URL <https://link.aps.org/doi/10.1103/PhysRevA.109.023709>
- [55] Aspelmeyer M, Kippenberg T J and Marquardt F 2014 *Rev. Mod. Phys.* **86**(4) 1391–1452 URL <https://link.aps.org/doi/10.1103/RevModPhys.86.1391>
- [56] Bariani F, Seok H, Singh S, Vengalattore M and Meystre P 2015 *Phys. Rev. A* **92**(4) 043817 URL <https://link.aps.org/doi/10.1103/PhysRevA.92.043817>
- [57] Motazedifard A, Bemani F, Naderi M H, Roknizadeh R and Vitali D 2016 *New Journal of Physics*

- 18 073040 URL <https://dx.doi.org/10.1088/1367-2630/18/7/073040>
- [58] Allahverdi H, Motazedifard A, Dalafi A, Vitali D and Naderi M H 2022 *Phys. Rev. A* **106**(2) 023107 URL <https://link.aps.org/doi/10.1103/PhysRevA.106.023107>
- [59] Wimmer M H, Steinmeyer D, Hammerer K and Heurs M 2014 *Phys. Rev. A* **89**(5) 053836 URL <https://link.aps.org/doi/10.1103/PhysRevA.89.053836>
- [60] Sainadh U S and Kumar M A 2020 *Phys. Rev. A* **102**(6) 063523 URL <https://link.aps.org/doi/10.1103/PhysRevA.102.063523>
- [61] Chao S L, Yang Z, Zhao C S, Peng R and Zhou L 2021 *Opt. Lett.* **46** 3075–3078 URL <https://opg.optica.org/ol/abstract.cfm?URI=ol-46-13-3075>
- [62] Xu X and Taylor J M 2014 *Phys. Rev. A* **90**(4) 043848 URL <https://link.aps.org/doi/10.1103/PhysRevA.90.043848>
- [63] Zhang W Z, Han Y, Xiong B and Zhou L 2017 *New J. Phys.* **19** 083022 URL <https://dx.doi.org/10.1088/1367-2630/aa68d9>
- [64] Kuhn A G, Teissier J, Neuhaus L, Zerkani S, van Brackel E, Deléglise S, Briant T, Cohadon P F, Heidmann A, Michel C, Pinard L, Dolique V, Flamínio R, Taïbi R, Chartier C and Le Traon O 2014 *Applied Physics Letters* **104** 044102 ISSN 0003-6951 URL <https://doi.org/10.1063/1.4863666>
- [65] Holstein T and Primakoff H 1940 *Phys. Rev.* **58**(12) 1098–1113 URL <https://link.aps.org/doi/10.1103/PhysRev.58.1098>
- [66] Sharma S, Bittencourt V A S V, Karenowska A D and Kusminskiy S V 2021 *Phys. Rev. B* **103**(10) L100403 URL <https://link.aps.org/doi/10.1103/PhysRevB.103.L100403>
- [67] Tiablikov S V 2013 *Methods in the quantum theory of magnetism* (Springer)
- [68] Yuan H, Cao Y, Kamra A, Duine R A and Yan P 2022 *Physics Reports* **965** 1–74 ISSN 0370-1573 quantum magnonics: When magnon spintronics meets quantum information science URL <https://www.sciencedirect.com/science/article/pii/S0370157322000977>
- [69] Benguria R and Kac M 1981 *Phys. Rev. Lett.* **46**(1) 1–4 URL <https://link.aps.org/doi/10.1103/PhysRevLett.46.1>
- [70] Gardiner C W and Collett M J 1985 *Phys. Rev. A* **31**(6) 3761–3774 URL <https://link.aps.org/doi/10.1103/PhysRevA.31.3761>
- [71] Rueda A, Sedlmeir F, Collodo M C, Vogl U, Stiller B, Schunk G, Strekalov D V, Marquardt C, Fink J M, Painter O, Leuchs G and Schwefel H G L 2016 *Optica* **3** 597–604 URL <https://opg.optica.org/optica/abstract.cfm?URI=optica-3-6-597>
- [72] Kim B, Kurokawa H, Sakai K, Koshino K, Kosaka H and Nomura M 2023 *Phys. Rev. Appl.* **20**(4) 044037 URL <https://link.aps.org/doi/10.1103/PhysRevApplied.20.044037>
- [73] Xing F F, Qin L G, Tian L J, Wu X Y and Huang J H 2023 *Opt. Express* **31** 7120–7133 URL <https://opg.optica.org/oe/abstract.cfm?URI=oe-31-5-7120>
- [74] Weaver M J, Duivesteyn P, Bernasconi A C, Scharmer S, Lemang M, Thiel T C v, Hijazi F, Hensen B, Gröblacher S and Stockill R 2023 *Nature Nanotechnology* ISSN 1748-3395 URL <https://doi.org/10.1038/s41565-023-01515-y>
- [75] Rochman J, Xie T, Bartholomew J G, Schwab K C and Faraon A 2023 *Nature Communications* **14** 1153 ISSN 2041-1723 URL <https://doi.org/10.1038/s41467-023-36799-0>
- [76] Motazedifard A, Dalafi A, Bemani F and Naderi M H 2019 *Phys. Rev. A* **100**(2) 023815 URL <https://link.aps.org/doi/10.1103/PhysRevA.100.023815>
- [77] Lü X Y, Wu Y, Johansson J R, Jing H, Zhang J and Nori F 2015 *Phys. Rev. Lett.* **114**(9) 093602 URL <https://link.aps.org/doi/10.1103/PhysRevLett.114.093602>
- [78] Li J, Zhu S Y and Agarwal G S 2019 *Phys. Rev. A* **99**(2) 021801 URL <https://link.aps.org/doi/10.1103/PhysRevA.99.021801>
- [79] Zhang W, Wang D Y, Bai C H, Wang T, Zhang S and Wang H F 2021 *Opt. Express* **29** 11773–11783 URL <https://opg.optica.org/oe/abstract.cfm?URI=oe-29-8-11773>
- [80] Guo Q, Cheng J, Tan H and Li J 2023 *Phys. Rev. A* **108**(6) 063703 URL <https://link.aps.org/doi/10.1103/PhysRevA.108.063703>

- [81] Barbieri R, Cerdonio M, Fiorentini G and Vitale S 1989 *Physics Letters B* **226** 357–360 ISSN 0370-2693 URL <https://www.sciencedirect.com/science/article/pii/0370269389912094>
- [82] Crescini N, Alesini D, Braggio C, Carugno G, D’Agostino D, Di Gioacchino D, Falferi P, Gambardella U, Gatti C, Iannone G, Ligi C, Lombardi A, Ortolan A, Pengo R, Ruoso G and Taffarello L (QUAX Collaboration) 2020 *Phys. Rev. Lett.* **124**(17) 171801 URL <https://link.aps.org/doi/10.1103/PhysRevLett.124.171801>
- [83] Flower G, Bourhill J, Goryachev M and Tobar M E 2019 *Physics of the Dark Universe* **25** 100306 ISSN 2212-6864 URL <https://www.sciencedirect.com/science/article/pii/S2212686418301985>
- [84] Ruoso G, Lombardi A, Ortolan A, Pengo R, Braggio C, Carugno G, Gallo C S and Speake C C 2016 *Journal of Physics: Conference Series* **718** 042051 URL <https://dx.doi.org/10.1088/1742-6596/718/4/042051>
- [85] Barbieri R, Braggio C, Carugno G, Gallo C, Lombardi A, Ortolan A, Pengo R, Ruoso G and Speake C 2017 *Physics of the Dark Universe* **15** 135–141 ISSN 2212-6864 URL <https://www.sciencedirect.com/science/article/pii/S2212686417300031>
- [86] Qian H, Zuo X, Fan Z Y, Cheng J and Li J 2024 *Phys. Rev. A* **109**(1) 013704 URL <https://link.aps.org/doi/10.1103/PhysRevA.109.013704>
- [87] Zhao X D, Zhao X, Jing H, Zhou L and Zhang W 2013 *Phys. Rev. A* **87**(5) 053627 URL <https://link.aps.org/doi/10.1103/PhysRevA.87.053627>
- [88] Wuhler D, Rohling N and Belzig W 2022 *Phys. Rev. B* **105**(5) 054406 URL <https://link.aps.org/doi/10.1103/PhysRevB.105.054406>
- [89] Wuhler D, Rózsa L, Nowak U and Belzig W 2023 *Phys. Rev. Res.* **5**(4) 043124 URL <https://link.aps.org/doi/10.1103/PhysRevResearch.5.043124>

(a) Original path



Detector

Detector